Critical minerals at the Berg and Huckleberry porphyry deposits, British Columbia, using scanning electron microscopy-mineral liberation analysis (SEM-MLA)

Evan A. Orovan[1, a], Shane Ebert[2], Peter Baldazzi[3], Derek Saxton[3], and Dylan J. Goudie[4]

[1] British Columbia Geological Survey, Ministry of Mining and Critical Minerals, Victoria, BC, V8W 9N3
[2] Surge Copper Corp., Vancouver, BC, V7Y 1G5
[3] Imperial Metals Corporation, Vancouver, BC, VC6 3B6
[4] Core Research Equipment and Training (CREAIT) Network, Memorial University of Newfoundland, St. John's, NL, A1C 5S7
[a] corresponding author: Evan.Orovan@gov.bc.ca

Recommended citation: Orovan, E.A., Ebert, S., Baldazzi, P., Saxton, D., and Goudie, D.J., 2025. Critical minerals at the Berg and Huckleberry porphyry deposits, British Columbia, using scanning electron microscropy-mineral liberation analysis (SEM-MLA). In: Geological Fieldwork 2024, British Columbia Ministry of Mining and Critical Minerals, British Columbia Geological Survey Paper 2025-01, pp. 73-84.

Abstract

Scanning electron microscopy-mineral liberation analysis (SEM-MLA) on seven samples from the Berg and Huckleberry porphyry Cu-Mo deposits reveal a range of minerals containing elements that are on the 2024 Canadian critical mineral list. Both deposits are primary sources of copper (chalcopyrite) and molybdenum (molybdenite). In late veins, zinc (sphalerite), copper, and antimony (tetrahedrite) are predominant. These veins include minor concentrations of minerals containing bismuth, tellurium, palladium, manganese, and tungsten, elements that could conceivably be byproducts of primary commodity mining.

Keywords: Berg, Huckleberry, porphyry Cu-Mo deposits, critical minerals, mineral liberation analysis, SEM-MLA, Cretaceous, Eocene

1. Introduction

Critical minerals are essential for low-carbon technologies, including electric vehicles, renewable energy systems, batteries, and medical devices (e.g., Kreiner et al., 2023; NRCan, 2024a). As global energy systems transition to low-carbon alternatives, the demand for these minerals is increasing, making diversification of supply a priority (IEA, 2024; WEF, 2024). Of the nine metal mines that operated in British Columbia in 2024, seven are porphyry deposits (Clarke et al., 2025). The province typically accounts for close to half of the annual national copper production and is the only producer of molybdenum (Clarke et al., 2025), both elements on the 2024 version of the Canadian critical minerals list (NRCan, 2024b). Many porphyry systems also contain a variety of minor 'companion metals' (Mudd et al., 2014, 2017; Nassar et al., 2015) on the critical minerals lists of different jurisdictions (Hickin et al., 2023, 2024) that could conceivably be byproducts of primary commodity production (e.g., John and Taylor, 2016; IGF, 2023) such as platinum group elements (PGE), Re, Te, W, Zn, Bi, and rare earth elements (REE). The diversity of porphyry deposits across British Columbia, driven by variations in magma sources, tectonic settings, and hydrothermal environments, results in distinct mineralogical and geochemical characteristics at each deposit (Ledoux and Hart, 2021). Maximizing the potential of these deposits requires an inventory of critical minerals in these different porphyry systems. Scanning electron microscopy-mineral liberation analysis (SEM-MLA) is a tool to start building such an inventory by providing detailed mineralogical and textural data to establish where elements considered critical reside.

This paper presents the results of SEM-MLA work on seven samples from the Huckleberry Cu-Mo deposit (Cretaceous) and the Berg Cu-Mo deposit (Eocene) in northwestern British Columbia (Fig. 1) in an area that includes the territories of many Indigenous Nations. Despite being only 22 km apart, these deposits differ significantly in age, host intrusion compositions, and hydrothermal alteration styles. Herein we document the mineralogy and possible paragenesis of primary commodity (Cu and Mo) and potential companion elements in these deposits, contributing to a better understanding of how critical minerals might be distributed in other porphyry deposits.

2. Geologic setting

The Huckleberry and Berg deposits are in Stikine terrane, near its western boundary with the Coast Plutonic complex (Fig. 1). Stikine terrane was accreted to the western margin of Ancestral North America in the Middle Jurassic (e.g., Nelson and van Straaten, 2020; George et al., 2021; Nelson et al., 2022). The Coast Plutonic complex consists of granitic rocks that were emplaced during the Jurassic to Paleogene (Gehrels et al., 2009; Brown, 2020).

In the study area (Fig. 2), Hazelton Group rocks including Lower Jurassic submarine and subaerial volcanic rocks of the Telkwa Formation (MacIntyre et al., 1989; Barresi et al., 2015)

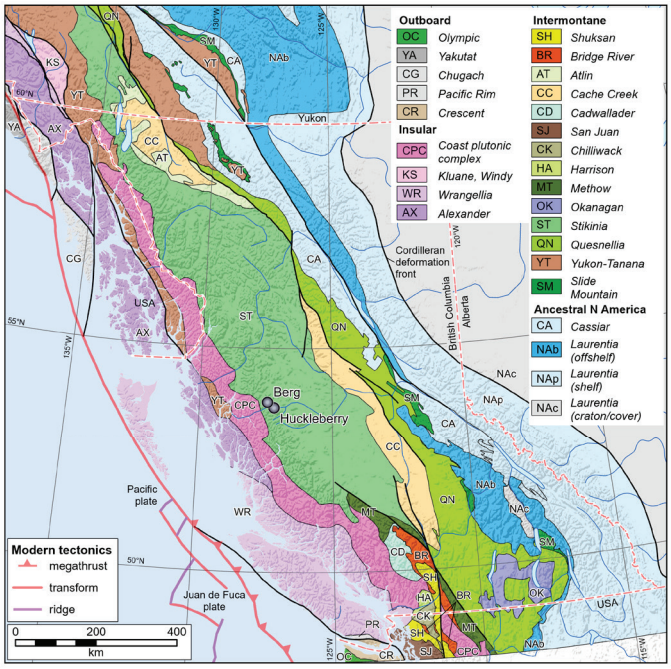

Fig. 1. Location of the Berg and Huckleberry Cu-Mo porphyry deposits, western Stikine terrane. Terranes modified from Colpron (2020).

and fossiliferous sedimentary rocks of the Smithers Formation (Tipper and Richards, 1976; Gagnon et al., 2012) are unconformably overlain by volcanic and sedimentary rocks of the Skeena Group (Early Cretaceous; Palsgrove and Bustin, 1991), which are in turn unconformably overlain by hornblende-bearing andesites of the Kasalka Group (Late Cretaceous; MacIntyre, 1976; Kim, 2020). The Bulkley intrusive suite (84-70 Ma; Carter, 1971, 1981), an age equivalent of the Kasalka Group, hosts numerous mineral occurrences, including Huckleberry, Whiting Creek, Bergette, Ox, and Seel (Fig. 2; Friedman and Jordan, 1997; Lepitre et al., 1998; Petersen, 2014; Ebert, 2020; Ogryzlo, 2020). The Bulkley intrusives have a calc-alkaline affinity suggesting magmatism was arc-related (MacIntyre, 1985; Petersen, 2014). The Nanika intrusive suite (58-45 Ma; Deyell et al., 2000; Diakow, 2006), consisting of granite, quartz monzonite, and granodiorite plutons and dikes, outcrop around the Berg deposit and are the youngest intrusions associated with known mineralization in the map area.

3. Deposit geology

3.1. Huckleberry calc-alkaline porphyry Cu-Mo deposit

Mining operations at Huckleberry ceased in August 2016, and the site is currently on care and maintenance status. The remaining combined historical and NI 43-101 compliant reserves and resources are estimated at 181.5 Mt at 0.32% Cu. Historical extraction from the deposit was 122.7 Mt, which yielded 0.498 Mt Cu, 3629 t Mo, 0.11 Moz Au, and 4.5 Moz Ag (Ogryzlo, 2020). The deposit consists of two primary mineralized areas (Main zone, East zone) which are spatially related to porphyritic granodiorite stocks of the Bulkley intrusive suite (Ogryzlo, 2020). Zircons from these stocks yielded U-Pb ages of 83.5 +0.3/-0.4 Ma (Main zone) and 83.5 ±0.3 Ma (East zone; Friedman and Jordan, 1997). The granodiorite stocks were emplaced into Lower Jurassic volcanic rocks of the Telkwa Formation (Fig. 2). In the Huckleberry area, these volcanic rocks are primarily lapilli tuffs and boulder conglomerates, which have undergone alteration to black biotite-magnetite hornfels, obscuring original fragmental textures (Ogryzlo, 2020). Further details on the geology, geochronology, hydrothermal alteration, mineralization, and structure of the Huckleberry deposit are available in studies by James (1976), MacIntyre (1976, 1985), Carter (1981), Jackson and Illerbrun (1995), Friedman and Jordan (1997), Ferbey and Levson (2001), Christensen and Connaughton (2016), and Ogryzlo (2020).

3.2. Berg calc-alkaline porphyry Cu-Mo deposit

The Berg deposit can be divided into an extensive supergene enrichment blanket and hypogene zone, both of which have been included in the NI 43-101 compliant Measured and Indicated resource of 1009 Mt at 0.23% Cu, 0.03% Mo, 4.62 g/t Ag, and 0.02 g/t Au (Ausenco Engineering Canada Inc., 2023). The deposit is centred on a composite porphyritic quartz monzonite stock (‘Berg stock’) of the Nanika intrusive suite, which was subdivided by Panteleyev (1976) into multiple textural phases, including porphyritic quartz monzonite (QMP), coarse-grained plagioclase-biotite-quartz porphyry (PBQP), medium-grained quartz-plagioclase porphyry (QPP), and late- to post-mineralization quartz-feldspar porphyry (QFP). Biotite from the Berg stock and whole-rock samples from the surrounding biotite hornfels were dated using K-Ar methods, yielding a mean age of 49.0 ±2.4 Ma (Carter, 1974). More detailed accounts of the geology, geochronology, hydrothermal alteration, mineralization, and structural features of the Berg deposit are provided by Panteleyev (1976, 1981), Heberlein and Godwin (1984), and Heberlein (1995).

4. Scanning electron microscopy-mineral liberation analysis (SEM-MLA)

4.1. SEM-MLA methods

Thin sections from seven representative rock samples (Table 1) were analyzed using an FEI Quanta 650F scanning electron microscope (SEM) equipped with MLA software (version 3) at the Scanning Electron Microscopy Laboratory, Micro Analysis Facility, CREAIT Network, Memorial University. Analyses were performed with an accelerating voltage of 25 kV and a beam current of 10 nA. The GXMAP (grain X-ray mapping) software mode was employed to generate mineral maps for each thin section. These maps were created by stitching together 1.5 by 1.5 mm frames, each with a resolution of 500 by 500 pixels (3 µm/pixel). Energy-dispersive X-ray spectroscopy (EDX) data was collected for each frame on a grid with 10-pixel (30 µm) spacing and a dwell time of 12 ms. The collected EDX spectra were compared to a reference library of mineral spectra to identify mineral phases

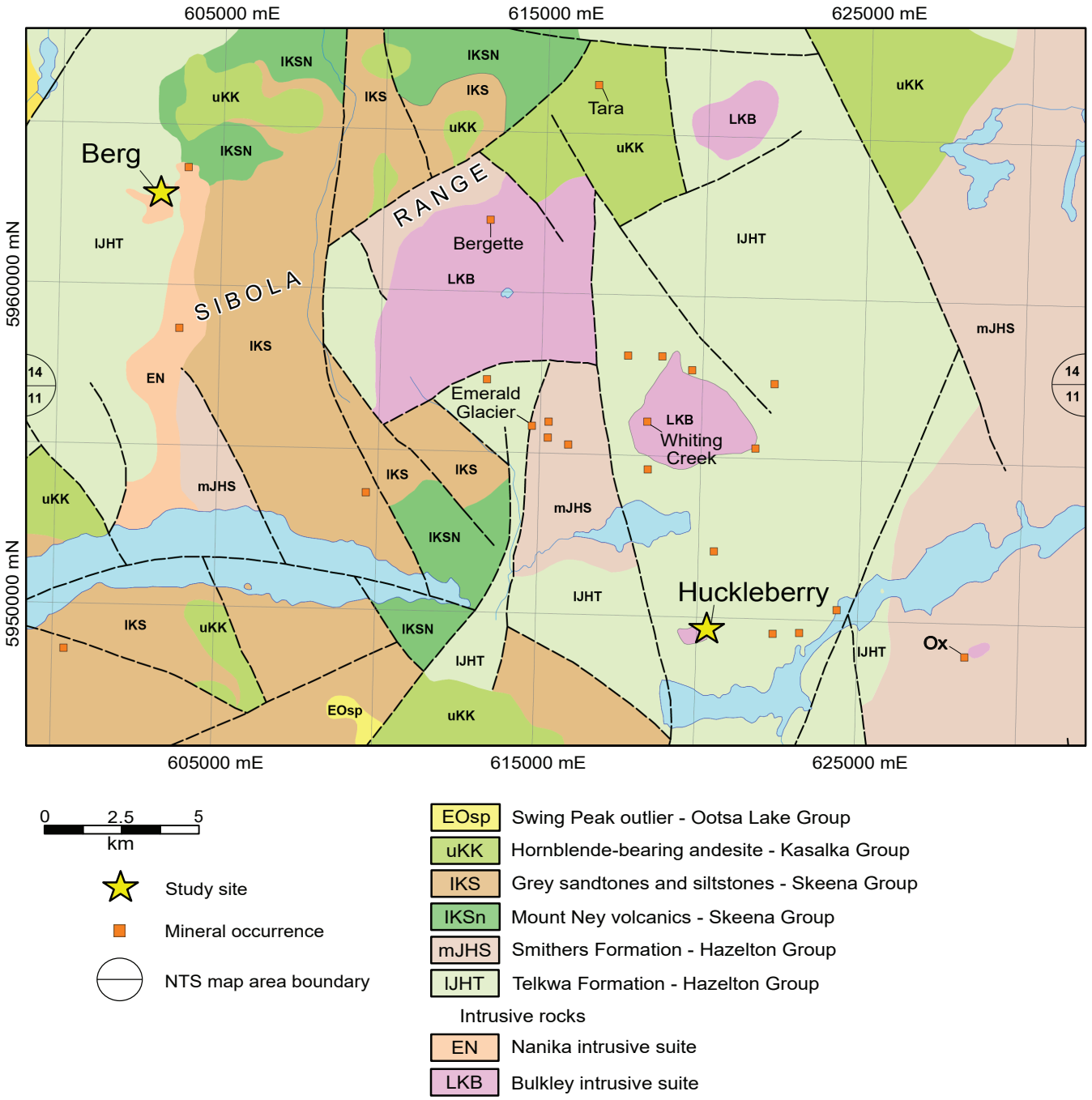

Fig. 2. Regional geology of the Berg and Huckleberry deposits (parts of NTS map sheets 93E/11, 14) and other mineral occurrences in the region. Simplified after Diakow (2006). Coordinates are UTM Zone 9N.

and quantify the mineralogical composition of each sample. For minerals referred to in this paper, mineral names, mineral formulae, main critical and precious metals, and mineral group are provided in Table 2.

To further process the MLA mineral maps and enable custom mineral groupings, a Python script was developed. This script decomposes mineral maps by segmenting and analyzing their colour composition. Each map was divided into smaller tiles, and unique colours within each tile were identified based on a predefined tolerance for colour similarity. For each identified colour, a binary mask was generated to highlight the corresponding regions, which were saved as transparent RGBA images. The processed tiles were then reassembled into full-resolution images, preserving the spatial arrangement of the original mineral map. This automated script facilitates the generation of stitched colour-separated layers, where each colour represents a unique mineral phase. These individual layers can be combined to create customized mineral groupings, providing an adaptable tool for robust mineralogical analyses.

Table 1. Samples referred to in text and figures. Coordinates are drill collar locations.

ID	Sample ID	Drill hole	Depth (m)	Lat.	Long.	Deposit
D23EOR-1-36	D23EOR-1-36	H20E-416	504	53.677060	-127.163354	Huckleberry
D23EOR-3-6	D23EOR-3-6	H20E-418	574	53.676418	-127.164570	Huckleberry
D23EOR-14-5	D23EOR-14-5	H20E-417	347	53.674476	-127.178911	Huckleberry
D23EOR-14-2	D23EOR-14-2	H20E-417	332	53.674476	-127.178911	Huckleberry
D23EOR-16-11	D23EOR-16-11	BRG23-244	365	53.798712	-127.428614	Berg
D23EOR-16-15B	D23EOR-16-15	BRG23-244	278	53.798712	-127.428614	Berg
D23EOR-18-1A	D23EOR-18-1	BRG23-245	304	53.803994	-127.440018	Berg

Table 2. Minerals, mineral formulae, and metals discussed in text and figures.

Mineral group	Mineral	Mineral formula	Critical (and other) metals	Observed at Huckleberry	Observed at Berg
Carbonate	Mn ankerite	$CaMn(CO_3)_2$	Mn		x
Carbonate	Mn calcite	$MnCO_3$	Mn		x
Sulpharsenide	Arsenopyrite	FeAsS	As		x
Sulpharsenide	Enargite	Cu_3AsS_4	Cu, As		x
Sulphosalt	Cosalite	$Pb_2Bi_2S_5$	Bi	x	x
Sulphosalt	Pyrargyrite	Ag_3SbS_3	Ag, Sb		x
Sulphosalt	Tetrahedrite	$(Cu,Fe)_{12}Sb_4S_{13}$	Cu, Sb	x	x
Sulphide	Acanthite	Ag_2S	Ag		x
Sulphide	Bismuthinite	Bi_2S_3	Bi	x	x
Sulphide	Bornite	Cu_5FeS_4	Cu	x	x
Sulphide	Chalcocite	Cu_2S	Cu		x
Sulphide	Chalcopyrite	$CuFeS_2$	Cu	x	x
Sulphide	Molybdenite	MoS_2	Mo	x	x
Sulphide	Sphalerite	ZnS	Zn	x	x
Telluride	Altaite	PbTe	Te	x	
Telluride	Hessite	Ag_2Te	Ag, Te		x
Telluride	Michenerite	PdBiTe	Pd, Bi, Te	x	
Telluride	Tellurobismuthinite	Bi_2Te_3	Bi, Te		x
Tungstate	Scheelite	$CaWO_4$	W	x	
Tungstate	Wolframite	$(Fe,Mn)WO_4$	W		x

4.2. SEM-MLA results

4.2.1. Huckleberry Cu-Mo porphyry deposit

Examination of four Huckleberry deposit vein samples indicates a possible paragenetic sequence. What appears to be an early banded quartz-anhydrite vein contains epitaxial molybdenite as the sole sulphide phase (Figs. 3a, c, d). Chalcopyrite, pyrite, and minor amounts of galena and pyrrhotite are observed as disseminations in the adjacent wall rock, but with no clear genetic relationship with the vein (Figs. 3a, c, d). A thin halo of plagioclase (<5 mm thick) surrounds the quartz-anhydrite-molybdenite-vein, highlighting localized alteration.

Chalcopyrite-pyrite-calcite-anhydrite veins (Figs. 3e-g) crosscut the early quartz-anhydrite-molybdenite veins and exhibit selvages of anhydrite-magnetite-quartz and vein halos of quartz-Mg-chlorite (Figs. 3e-f). Trace amounts of pyrrhotite, galena, sphalerite, and tetrahedrite occur throughout these veins, although their relationship to the main mineralizing event remains ambiguous.

Pyrite-quartz-calcite-ankerite veins feature halos of quartz-muscovite-pyrite alteration (Fig. 4). These veins are apparently sporadic throughout the Huckleberry East zone and have been observed to crosscut earlier formed chalcopyrite-pyrite veins. The pyrite in these veins contains inclusions of chalcopyrite, galena, scheelite, bismuthinite, cosalite, bornite, tetrahedrite,

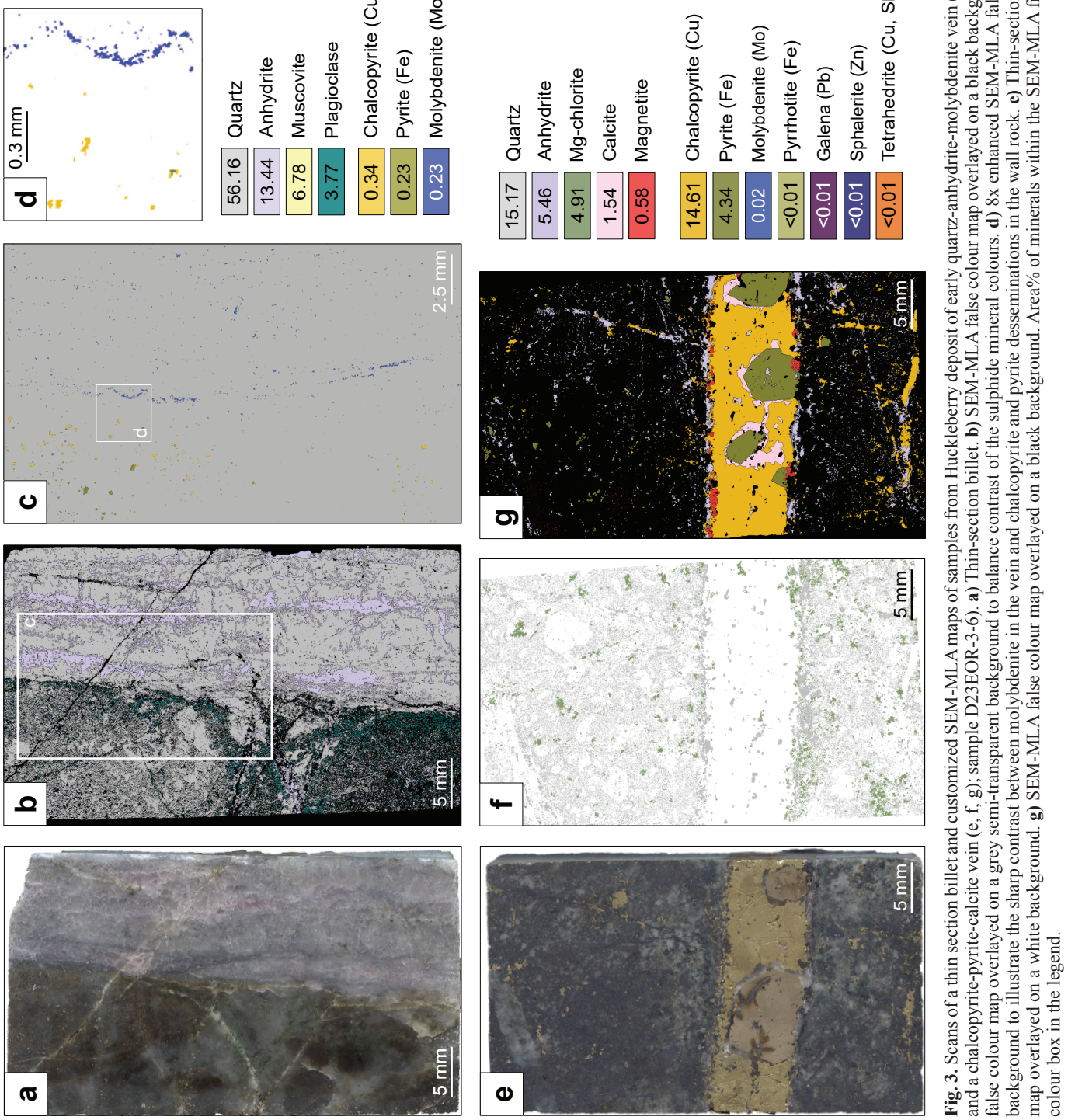

Fig. 3. Scans of a thin section billet and customized SEM-MLA maps of samples from Huckleberry deposit of early quartz-anhydrite-molybdenite vein (a, b, c, d); sample D23EOR-1-36) and a chalcopyrite-pyrite-calcite vein (e, f, g); sample D23EOR-3-6). **a)** Thin-section billet. **b)** SEM-MLA false colour map overlayed on a black background. **c)** 2x enhanced SEM-MLA false colour map overlayed on a grey semi-transparent background to balance contrast of the sulphide mineral colours. **d)** 8x enhanced SEM-MLA false colour map overlayed on white background to illustrate the sharp contrast between molybdenite in the vein and chalcopyrite and pyrite desseminations in the wall rock. **e)** Thin-section billet. **f)** SEM-MLA false colour map overlayed on a white background. **g)** SEM-MLA false colour map overlayed on a black background. Area% of minerals within the SEM-MLA field is indicated in the appropriate colour box in the legend.

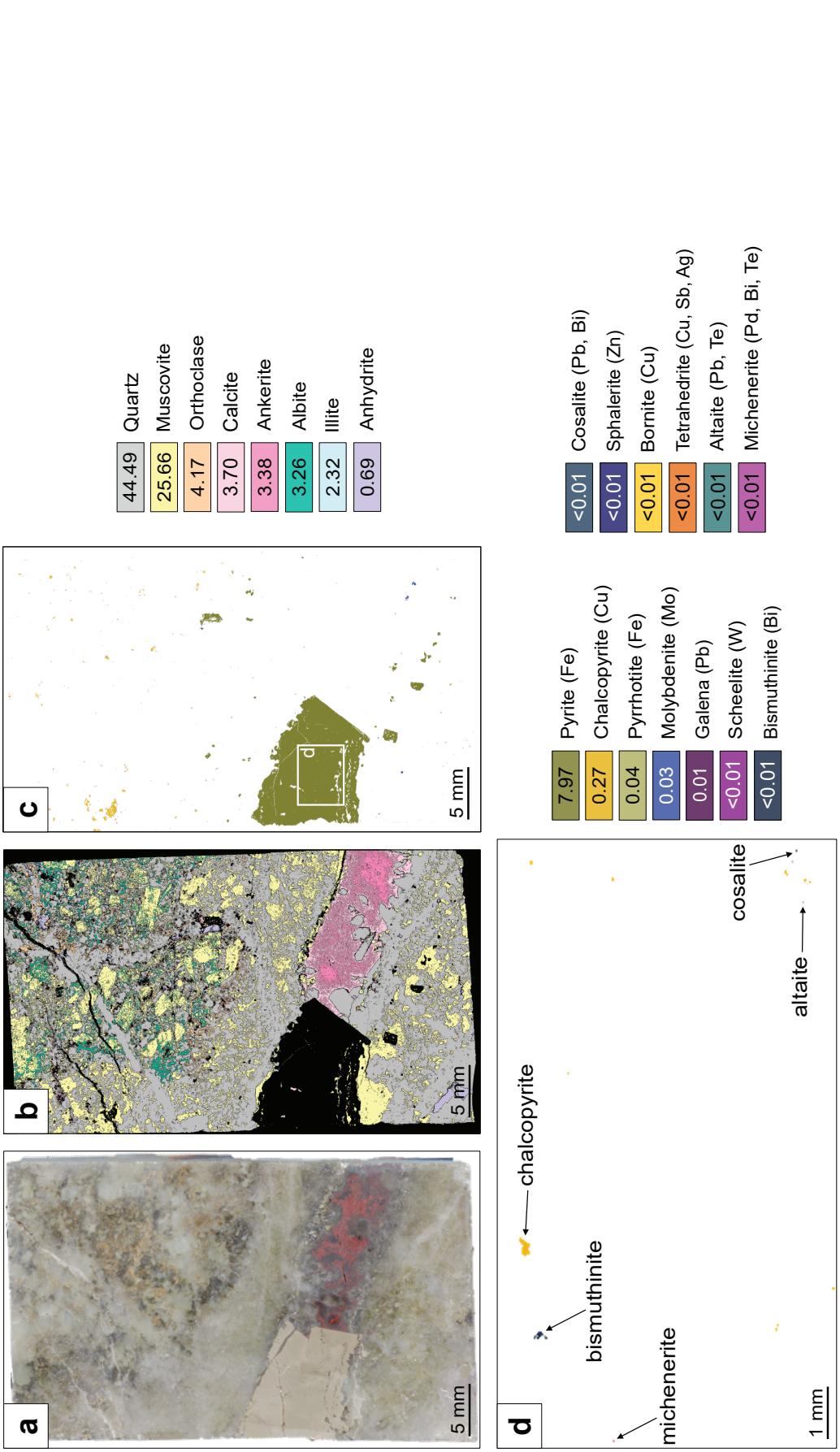

Fig. 4. Scan of a thin section billet and customized SEM-MLA maps of sample D23EOR-14-5 from the Huckleberry deposit of a pyrite-carbonate-quartz vein. **a)** Thin-section billet. **b)** SEM-MLA false colour map overlayed on a black background. **c)** SEM-MLA false colour map overlayed on a white background. **d)** Enhanced SEM-MLA false colour map with the bounding box show in panel c), overlayed on a white background. Area% of minerals within the SEM-MLA field is indicated in the appropriate colour box in the legend.

altaite, and michenerite, suggesting a more complex mineralizing environment compared with the older veins with predominantly chalcopyrite and molybdenite. Late anhydrite-sphalerite veins (Fig. 5) are observed to crosscut veins with predominantly pyrite. Sphalerite within these veins contains inclusions of galena, chalcopyrite, cosalite, and altaite and some of these minerals are interpreted to infill fractures in earlier-formed pyrite (Fig. 5c).

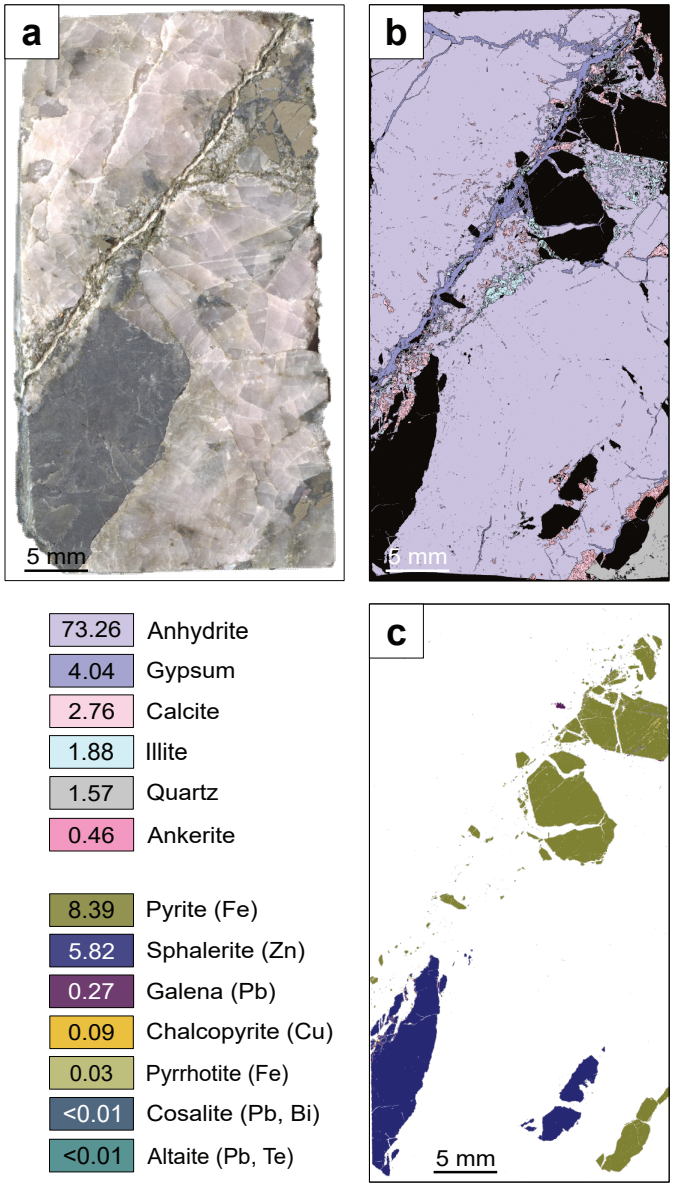

Fig. 5. Scan of a thin section billet and customized SEM-MLA maps of sample D23EOR-14-2 from the Huckleberry deposit of an anhydrite-sphalerite vein. **a)** Thin-section billet. **b)** SEM-MLA false colour map overlayed on a black background. **c)** SEM-MLA false colour map overlayed on a white background. Area% of minerals within the SEM-MLA field is indicated in the appropriate colour box in the legend. Cosalite and altaite occur as inclusions within sphalerite, but they are too sparse and small to show.

4.2.2. Berg porphyry Cu-Mo deposit

The SEM-MLA maps of three samples from the Berg Cu-Mo deposit also indicate early to late stages of mineralization (Figs. 6-8). Early banded quartz-molybdenite-anhydrite veins lack other sulphide phases and are surrounded by a muscovite-orthoclase halo (Fig. 6). These veins are crosscut by pyrite-anhydrite-ankerite-illite veins (Fig. 6). The pyrite within these crosscutting veins contains inclusions of chalcopyrite, sphalerite, galena, and cosalite (Fig. 6d); the associated ankerite exhibits Mn-rich carbonate zoning (Fig. 6b).

A late hydrothermal vein shows distinct symmetrical banding. The outer layers consist of euhedral quartz walls transitioning inward to zoned ankerite, followed by colloform sphalerite-pyrite bands (Fig. 7). The sphalerite is mantled by chalcopyrite, galena, enargite, and tetrahedrite (Figs. 7c, e). Toward the vein's core, carbonate layers transition into anhydrite-barite-celestine (Figs. 7c, d), the final phases in this vein generation. Trace amounts of hessite, arsenopyrite, bismuthinite, tellurobismuthinite, wolframite, and acanthite are distributed throughout the vein (Fig. 7). The youngest vein stage identified at Berg in this study comprises intergrown tetrahedrite, pyrite, enargite, chalcopyrite, galena, and sphalerite, with trace occurrences of cosalite, bornite, molybdenite, hessite, pyrargyrite, arsenopyrite, acanthite, tellurobismuthinite, bismuthinite, wolframite, and chalcocite (Fig. 8).

5. Discussion

5.1. Critical minerals at Huckleberry

The Huckleberry deposit displays the mineralogical traits typical of calc-alkaline Cu-Mo porphyry systems as described elsewhere (e.g., Seedorff et al., 2005; Sillitoe, 2010). Chalcopyrite and molybdenite are predominant in the early and main stages and host Cu and Mo, both on the 2024 version of the Canadian critical minerals list (NRCan, 2024b). Because incorporation of Re in molybdenite is common in other porphyry deposits (Reich et al., 2013; John and Taylor, 2016) we speculate that Re may be a companion element at Huckleberry.

The transitional vein stage, interpreted as phyllic based on quartz-muscovite-pyrite alteration halos (cf. Harris and Golding, 2002; Sillitoe, 2010), contains critical metal-bearing sulphides (sphalerite, bornite), sulphosalts (tetrahedrite, bismuthinite, cosalite), tungstates (scheelite), and tellurides (altaite, michenerite) underscoring the mineralogical complexity of the deposit. These minerals contain trace quantities of metals commonly on critical mineral lists (W, Bi, Zn, Cu, Sb, Te, and Pd).

In the youngest ore-bearing vein stage, sphalerite is the primary critical metal-bearing mineral with trace cosalite and altaite inclusions. Although rare, these veins host Zn, Bi, and Te. Previous studies establish that sphalerite from porphyry deposits may contain significant quantities of In, Ga, Ge, W, Cu, Ag, and Cd (Beaucamp et al., 2024).

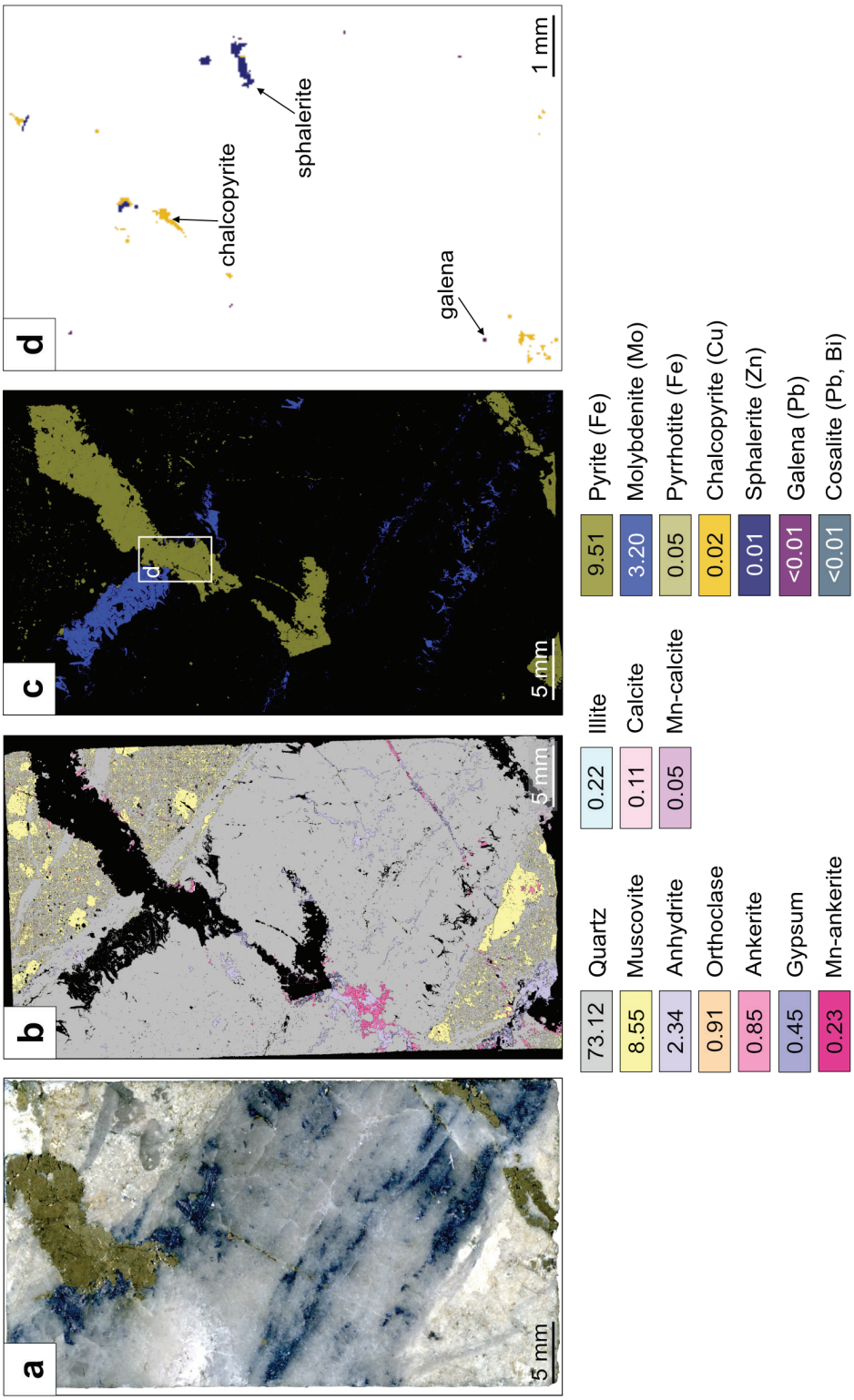

Fig. 6. Scan of a thin section billet and customized SEM-MLA maps of sample D23EOR-16-11 from the Berg deposit of an early quartz-molybdenite-anhydrite vein crosscut by a pyrite-anhydrite-carbonate vein. **a)** Thin-section billet. **b)** SEM-MLA false colour map overlayed on a black background. **c)** SEM-MLA false colour map overlayed on a black background. **d)** 5x enhanced SEM-MLA false colour map with the bounding box shown in panel c), overlayed on a white background. Area% of minerals within the SEM-MLA field is indicated in the appropriate colour box in the legend.

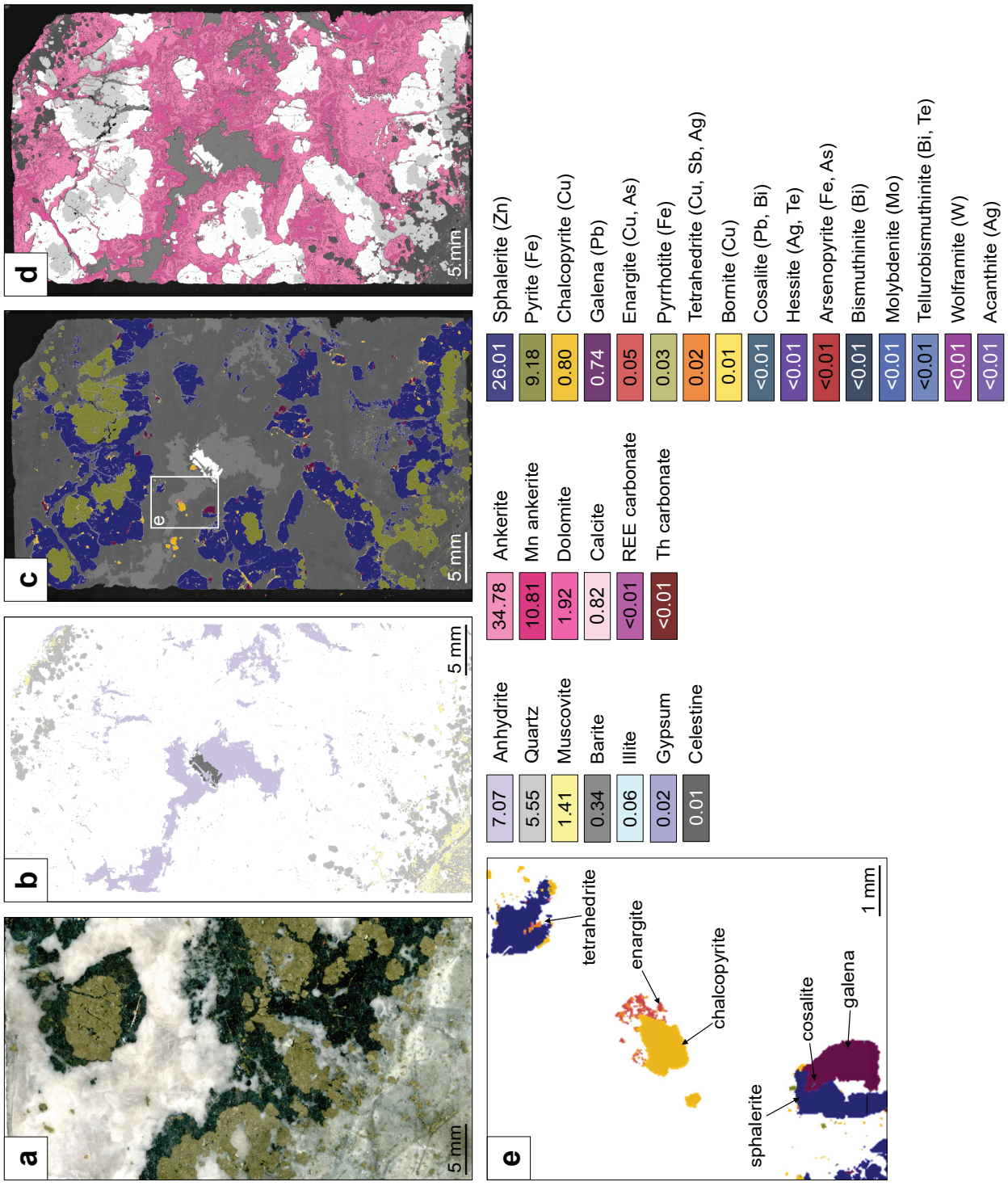

Fig. 7. Scan of a thin section billet and customized SEM-MLA maps of sample D23EOR-16-15B from the Berg deposit of a late-stage carbonate-sphalerite-sulfate vein. **a)** Thin-section billet. **b)** SEM-MLA false colour map overlayed on a white background. **c)** SEM-MLA false colour map overlayed on backscattered electron (BSE) image. **d)** SEM-MLA false colour map overlayed on a BSE image. **e)** 5x enhanced SEM-MLA false colour map with the bounding box shown in panel e), overlayed on a white background. Area% of minerals within the MLA field is indicated in the appropriate colour box in the legend.

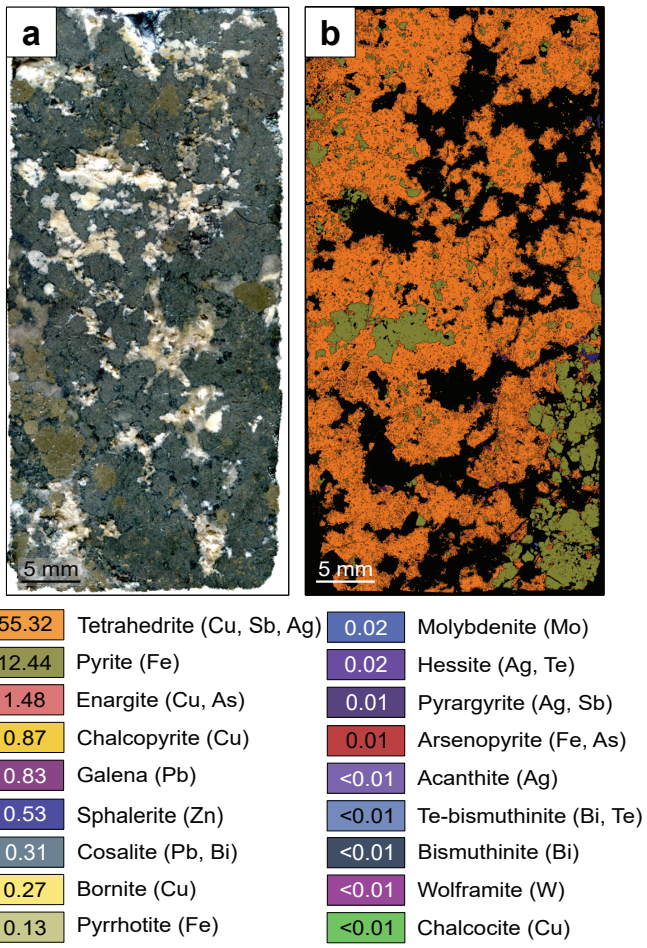

Fig. 8. Scan of a thin section billet and customized SEM-MLA maps of sample D23EOR-18-1A from the Berg deposit from a late-stage tetrahedrite-pyrite-carbonate vein. **a)** Thin-section billet. **b)** SEM-MLA false colour map overlayed on a black background. Area% of minerals within the SEM-MLA field is indicated in the appropriate colour box in the legend.

5.2. Critical minerals at Berg

Panteleyev (1981) identified five hypogene vein stages at the Berg deposit. We recognized three representative vein types, encompassing the middle stages specified by Panteleyev (1981). Early quartz-molybdenite-anhydrite veins contain predominantly molybdenite. The transitional pyrite-anhydrite-carbonate vein crosscuts earlier veins and hosts minor chalcopyrite, sphalerite, galena, and cosalite, with Zn, Cu, and Bi. Similar to Huckleberry, late veins display more complex mineralogy, with colloform banded sphalerite veins showing zoning of Mn-rich carbonate minerals (Fig. 7). Sulphides include sphalerite, chalcopyrite, enargite, bornite, and molybdenite with trace amounts of associated sulphosalts (tetrahedrite, cosalite), tellurides (hessite, tellurobismuthinite), tungstates (wolframite), and sulpharsenides (arsenopyrite), incorporate Zn, Cu, As, Sb, Mo, Te, Bi, and W. These late veins also contain tetrahedrite, enargite, minor chalcopyrite and sphalerite, and trace amounts sulphosalts and tellurides, hosting an array of elements, including Cu, Sb, As, Zn, Bi, Mo, Te, and W (Table 2).

6. Conclusion

The Berg and Huckleberry deposits display the mineralogical complexity of calc-alkaline porphyry Cu-Mo systems. Chalcopyrite and molybdenite are the primary ore minerals in both deposits. The SEM-MLA results reveal a transition from early veins with predominantly chalcopyrite and molybdenite to later veins with sphalerite and galena (containing Zn). These late veins contain a variety of minor and trace phases with metals that are on the 2024 Canadian critical minerals list (NRCan, 2024b), including Te, As, Bi, Mn, Sb, Pd, and W.

Future studies should incorporate bulk rock geochemistry and micro-analytical techniques, such as electron probe micro-analysis (EPMA) and laser ablation inductively coupled plasma mass spectrometry (LA-ICP-MS), to quantify trace critical metals in sulphides and other minerals.

Acknowledgments

This project benefited from field assistance by Katya Zaborniak and office support by Kirsty Hooker. Constructive reviews and comments by Steve Piercey, Don MacIntyre, and Bram van Straaten helped improve the paper.

References cited

Ausenco Engineering Canada Inc., 2023. Berg project NI 43-101 technical report and preliminary economic assessment. Available at: <www.sedar.com>

Barresi, T., Nelson, J.L., Dostal, J., and Friedman, R.M., 2015. Evolution of the Hazelton arc near Terrace, British Columbia: stratigraphic, geochronological, and geochemical constraints on a Late Triassic-Early Jurassic arc and Cu-Au porphyry belt. Canadian Journal of Earth Sciences, 52, 466-494.

Beaucamp, C.M.E., Gammons, C.H., Thompson. J.M., and Lowers, H.A., 2024. Fluorescent sphalerite rich in tungsten, copper, gallium, silver, and other elements from the Cordilleran-style, polymetallic veins of Philipsburg, Montana. Ore Geology Reviews, 173, article 106267. <https://doi.org/10.1016/j.oregeorev.2024.106267>

Brown, E.H., 2020. Magma loading in the southern Coast Plutonic complex, British Columbia and Washington. Lithosphere, article 8856566. <https://doi.org/10.2113/2020/8856566>

Carter, N.C., 1971. Porphyry copper and molybdenum deposits of west-central British Columbia. In: Geology, Exploration, and Mining in British Columbia 1971, British Columbia Ministry of Energy, Mines and Petroleum Resources, pp. 271-274.

Carter, N.C., 1974. K-Ar dating of the Berg stock. In: Geological Fieldwork 1974, British Columbia Ministry of Energy, Mines and Petroleum Resources, British Columbia Geological Survey Paper 1975-1, pp. 41-42.

Carter, N.C., 1981. Porphyry copper and molybdenum deposits, west-central British Columbia. British Columbia Ministry of Energy, Mines and Petroleum Resources, British Columbia Geological Survey Bulletin 64, 150 p.

Christensen, K., and Connaughton, G.R., 2016. Technical report on the Main Zone optimization, Huckleberry Mine, Omineca Mining Division, British Columbia, Canada. Available at: <www.sedar.com>

Clarke, G., Northcote, B.K., Corcoran, N.L., Pothorin, C., Heidarian, H., and Hancock, K., 2025. Exploration and Mining in British Columbia, 2024: A summary. In: Provincial Overview of Exploration and Mining in British Columbia, 2024.

British Columbia Ministry of Mining and Critical Minerals, British Columbia Geological Survey Information Circular 2025-01, pp. 1-60.

Colpron, M., 2020. Yukon Terranes-A digital atlas of terranes for the northern Cordillera. Yukon Geological Survey. <data.geology.gov.yk.ca/Compilation/2#InfoTab>

Deyell, C.L., Thompson, J.F.H., Friedman, R.M., and Groat, L.A., 2000. Age and origin of advanced argillic alteration zones and related exotic limonite deposits in the Limonite Creek area, central British Columbia. Canadian Journal of Earth Sciences, 37, 1093-1107.

Diakow, L.J., 2006. Geology of the Tahtsa Ranges between Eutsuk Lake and Morice Lake (93E/8, 9, 10, 15; 93L/12, 13, 14), west-central British Columbia. British Columbia Ministry of Energy, Mines and Petroleum Resources, British Columbia Geological Survey Open File 2006-11.

Ebert, S., 2020. The Seel and Ox porphyry deposits, Ootsa property, west-central British Columbia. In: Porphyry Deposits of the Northwestern Cordillera of North America, 2nd Edition, Schroeter, T.G., (Ed.), Canadian Institute of Mining, Metallurgy and Petroleum, Special Volume 57, pp. 327-340.

Ferbey, T., and Levson, V.M., 2001. Quaternary geology and till geochemistry of the Huckleberry Mine area. In: Geological Fieldwork 2000, British Columbia Ministry of Energy and Mines, British Columbia Geological Survey Paper 2001-1, pp. 397-409.

Friedman, R.M., and Jordan, S.R., 1997. U-Pb ages for intrusive rocks at the Huckleberry porphyry copper deposit, Tahtsa Lake district, Whitesail Lake map area, west-central British Columbia. In: Geological Fieldwork 1996, British Columbia Ministry of Employment and Investment, British Columbia Geological Survey Paper 1997-1, pp. 219-226.

Gagnon, J.-F., Barresi, T., Waldron, J.W.F., Nelson, J.L., Poulton, T.P., and Cordey, F., 2012. Stratigraphy of the upper Hazelton Group and the Jurassic evolution of the Stikine terrane, British Columbia. Canadian Journal of Earth Sciences, 49(9), 1027-1052.

Gehrels, G.E., Rusmore, M.E., Woodsworth, G.J., Crawford, M.L., Andronicos, C.L., Hollister, L.S., Patchett, P.J., Ducea, M.N., Butler, R.F., Klepeis, K.A., and Davidson, C., 2009. U-Th-Pb geochronology of the Coast Mountains batholith in north-coastal British Columbia: Constraints on age and tectonic evolution. Geological Society of America Bulletin, 121, 1341-1361.

George, L.L., Nelson, J.L., and Friedman, R.M., 2021. U-Pb geochronology and tectonic significance of the Hazelton Group in the Iskut River area, northwestern British Columbia. Canadian Journal of Earth Sciences, 58, 1-24.

Harris, A.C., and Golding, S.D., 2002. New evidence of magmatic-fluid-related phyllic alteration: Implications for the genesis of porphyry Cu deposits. Geology, 30, 335-338.

Heberlein, D., 1995. Geology and supergene processes: Berg copper-molybdenum porphyry, west-central British Columbia. In: Porphyry Deposits of the Canadian Cordillera, Schroeter, T.G., (Ed.), Canadian Institute of Mining, Metallurgy and Petroleum, Special Volume 46, pp. 304-312.

Heberlein, D., and Godwin, C., 1984. Hypogene alteration at the Berg porphyry copper-molybdenum property, north-central British Columbia. Economic Geology, 79, 901-918.

Hickin, A.S., Orovan, E.A., Brzozowski, M.J., McLaren, K., Shaw, K., and Van der Vlugt, J., 2023. Critical minerals in British Columbia: An atlas of occurrences and producing mines, 2024. British Columbia Ministry of Energy, Mines and Low Carbon Innovation, British Columbia Geological Survey Open File 2023-02, 102 p.

Hickin, A.S., Ootes, L., Orovan, E.A., Brzozowski, M.J., Northcote, B.K., Rukhlov, A.S., and Bain, W.M., 2024. Critical minerals and mineral systems in British Columbia. In: Geological Fieldwork 2023, British Columbia Ministry of Energy, Mines and Low Carbon Innovation, British Columbia Geological Survey Paper 2024-01, pp. 13-51.

IEA (International Energy Agency, 2024. Global critical minerals outlook 2024. <https://www.iea.org/reports/global-critical-minerals-outlook-2024> (last accessed December 5, 2024).

IGF (Intergovernmental Forum on Mining, Minerals, Metals, and Sustainable Development), 2023. Searching for critical minerals? How metals are produced and associated together, 30 p. <https://www.igfmining.org/resource/searching-for-critical-minerals-how-metals-are-produced-and-associated-together/> (last accessed December 14, 2024).

Jackson, M.R., and Illerbrun, K.L., 1995. Geology and mineralization of the Huckleberry porphyry copper deposit, Tahtsa Lake district, west-central British Columbia. In: Porphyry Deposits of the Northwestern Cordillera of North America, Schroeter, T.G., (Ed.), Canadian Institute of Mining, Metallurgy and Petroleum, Special Volume 46, pp. 313-324.

James, D.H., 1976. Huckleberry porphyry copper-molybdenum deposit. In: Porphyry Deposits of the Canadian Cordillera, Sutherland Brown, A., (Ed.), Canadian Institute of Mining and Metallurgy, Special Volume 15, pp. 284-288.

John, D.A., and Taylor, R.D., 2016. By-products of porphyry copper and molybdenum deposits. In: Critical Mineral Resources of the United States-Economic and Environmental Geology and Prospects for Future Supply, Schulz, K.J., DeYoung, J.H., Seal, R.R., and Bradley, D.C., (Eds.), U.S. Geological Survey Professional Paper 1802, pp. 323-354.

Kim, R.S.Y., 2020. Evolution of Late Cretaceous Kasalka Group volcanics, Nechako Plateau, central British Columbia. Unpublished M.Sc. thesis, University of British Columbia, Vancouver, Canada, 148 p.

Kreiner, D.C., Hammerstrom, J., and Day, W., 2023. Critical minerals for a carbon-neutral future. <https://www.usgs.gov/publications/critical-minerals-a-carbon-neutral-future> (last accessed December 5, 2024).

Ledoux, T.J., and Hart, C.J.R., 2021. Evolution of the southern Quesnel arc: potential to distinguish variability in magmatic porphyry fertility, south-central British Columbia (NTS 082E, L, 092H, I, P, 093A, B). In: Geoscience BC Summary of Activities 2020, Geoscience BC Report 2021-01, pp. 75-90.

Lepitre, M.E., Mortensen, J.K., Friedman, R.M., and Jordan, S.J., 1998. Geology and U-Pb geochronology of intrusive rocks associated with mineralization in the northern Tahtsa Lake district, west-central British Columbia. In: Geological Fieldwork 1997, British Columbia Ministry of Employment and Investment, British Columbia Geological Survey Paper 1998-1, pp. 32-1 to 32-8.

MacIntyre, D.G., 1976. Evolution of Upper Cretaceous volcanic and plutonic centers and associated porphyry copper occurrences Tahtsa Lake area, British Columbia. Ph.D. thesis, University of Western Ontario, 148 p.

MacIntyre, D.G., 1985. Geology and mineral deposits of the Tahtsa Lake district, west-central British Columbia. British Columbia Ministry of Energy, Mines and Petroleum Resources, British Columbia Geological Survey Bulletin 75, 82 p.

MacIntyre, D.G., Desjardins, P.J., and Tercier, P.E., 1989. Geology of the Smithers and Terrace areas, west-central British Columbia. British Columbia Ministry of Energy, Mines and Petroleum Resources, British Columbia Geological Survey Open File 1989-4, 1:250,000 scale.

Mudd, G.M., Yellishetty, M., Reck, B.K., and Graedel, T.E., 2014. Quantifying the recoverable resources of companion metals: A preliminary study of Australian mineral resources. Resources, 3, 657-671. <https://doi.org/10.3390/resources3040657>

Mudd, G.M., Jowitt, S.M., and Werner, T.T., 2017. The world's by-product and critical metal resources part I: Uncertainties, current reporting practices, implications and grounds for optimism. Ore Geology Reviews, 86, 924-938.

Nassar, N.T., Graedel T.E., and Harper, E.M., 2015. By-product metals are technologically essential but have problematic supply. Science Advances, article 1,e1400180. <https://doi.org/10.1126/sciadv.1400180>

Nelson, J.L., and van Straaten, B.I., 2020. Geology and mineral deposits of the Quesnel terrane, British Columbia. In: Geology of the Canadian Cordillera, Colpron, M., Nelson, J.L., and Friedman, R.M., (Eds.), Geological Association of Canada, Special Paper 49, pp. 159-194.

Nelson, J.L., van Straaten, B.I., and Friedman, R.M., 2022. Tectonic evolution of the Stikine terrane, British Columbia. In: Tectonic Evolution of the Canadian Cordillera, Colpron, M., Nelson, J.L., and Friedman, R.M., (Eds.), Geological Association of Canada, Special Paper 50, pp. 195-224.

NRCan (Natural Resources Canada), 2024a. Canadian Critical Minerals Strategy Annual Report 2024. <https://www.canada.ca/en/campaign/critical-minerals-in-canada/canadas-critical-minerals-strategy/canadian-critical-minerals-strategy-annual-report-2024.html> (last accessed December 5, 2024).

NRCan (Natural Resources Canada), 2024b. Critical Minerals List. Government of Canada. <https://www.canada.ca/en/campaign/critical-minerals-in-canada/critical-minerals-an-opportunity-for-canada.html> (last accessed December 27, 2024).

Ogryzlo, P.L., 2020. Huckleberry porphyry copper-molybdenum deposit. In: Porphyry Deposits of the Northwestern Cordillera of North America, Schroeter, T.G., (Ed.), Canadian Institute of Mining, Metallurgy and Petroleum, Special Volume 46, pp. 290-303.

Palsgrove, R.J., and Bustin, R.M., 1991. Stratigraphy, sedimentology and coal quality of the Lower Skeena Group, Telkwa coalfield, central British Columbia, NTS 93L/11. British Columbia Ministry of Energy, Mines and Petroleum Resources, Paper 1991-2, 60 p.

Panteleyev, A., 1976. Geologic setting, mineralization, and aspects of zoning at the Berg porphyry copper-molybdenum deposit, central British Columbia. Unpublished Ph.D. thesis, University of British Columbia, 235 p.

Panteleyev, A., 1981. Berg porphyry copper-molybdenum deposit: Geologic setting, mineralization, zoning, and pyrite geochemistry. British Columbia Ministry of Energy, Mines and Petroleum Resources, Bulletin 66, 95 p.

Petersen, T.D., 2014. Geology and mineralization of the Bulkley intrusive suite, west-central British Columbia. In: Geological Fieldwork 2013, British Columbia Ministry of Energy and Mines, British Columbia Geological Survey Paper 2014-1, pp. 119-134.

Reich, M., Palacios, C., Barra, F., and Chryssoulis, S., 2013. “Invisible” silver in chalcopyrite and bornite from the Mantos Blancos Cu deposit, northern Chile. European Journal of Mineralogy, 25, 453-460. <https://doi.org/10.1127/0935-1221/2013/0025-2287>

Seedorff, E., Dilles, J.H., Proffett, J.M., Einaudi, M.T., Zurcher, L., Stavast, W.J.A., Johnson, D.A., and Barton, M.D., 2005. Porphyry deposits: Characteristics and origin of hypogene Features. In: Hedenquist, J.W., Thompson, J.F.H., Goldfarb, R.J., and Richards, J.P., (Eds.), Economic Geology, 100th Anniversary Volume, 251-298.

Sillitoe, R.H., 2010. Porphyry copper systems. Economic Geology, 105, 3-41.

Tipper, H.W., and Richards, T.A., 1976. Jurassic stratigraphy and history of north-central British Columbia. Geological Survey of Canada, Bulletin 270, 73 p.

WEF (World Economic Forum), 2024. Energy Transition: Securing Critical Minerals Needs Collective Action. <https://www.weforum.org/stories/2024/02/securing-critical-minerals-energy-transition-collective-action/> (last accessed December 5, 2024).